Sensitivity to Supernovae Average ν_x Temperature with Neutral Current Interactions in DUNE

Darcy A. Newmark¹ and Austin Schneider^{2, 1}

¹ Dept. of Physics, Massachusetts Institute of Technology, Cambridge, MA 02139, USA

² Los Alamos Laboratory, Los Alamos, NM 87545, USA

(Dated: April 4, 2023)

We explore a novel method for measuring the average temperature of the ν_x component in Type-II core-collapse supernovae. By measuring neutral current incoherent neutrino-Argon interactions in DUNE we can obtain spectral information for the combination of all active neutrino species. Combining this all-neutrino spectral information with detailed charged current measurements of the electron neutrino and electron anti-neutrino fluxes from DUNE and Hyper-Kamiokande, we can infer the average temperature for the remaining neutrino species in the ν_x component to within a factor two for most cases and to 30% for a small range of average ν_x temperatures. Due to the limited energy range of the emitted photons from incoherent neutral current interactions on Argon, the ν_x temperature reconstruction demonstrates a degeneracy in the one and two sigma credible regions. Furthermore, while large uncertainties on the NC cross-section penalize this measurement, we examined the efficacy of constraining NC cross-section uncertainties on improving ν_x measurements. We found that if additional measurements of B(M1 \uparrow) 1⁺ excited state transitions in Argon are able to reduce correlated cross section uncertainties from 15% to 7%, the size of the 1 σ allowed regions for T_{ν_x} becomes sample size limited, and approaches the case where there are no uncertainties on the cross-section.

I. INTRODUCTION

Type-II core-collapse supernovae events release approximately 10^{53} ergs of energy, carried away almost exclusively by neutrinos and antineutrinos of all flavors [1]. These neutrinos travel nearly unimpeded to Earth, where they can be detected. In 1987, two neutrino detectors on Earth measured 20 events within 13 seconds, which coincided with the release of energy from the collapse of SN1987A [1]. If a core collapse supernovae event were to occur within the Galaxy today, the many operating neutrino detectors would provide precise measurements of neutrino and antineutrino energy spectra. Such measurements are crucial for reconstructing the initial conditions of supernovae just before collapse, understanding their evolution, and modeling their collapse.

Large detectors such as the Deep Underground Neutrino Experiment (DUNE) and Hyper-Kamiokande (Hyper-K) will provide large sample measurements of ν_e and $\bar{\nu_e}$ charged current (CC) interactions, respectively, with excellent energy resolution [2, 3] However, the remaining neutrino species, summarized as ν_x , are below threshold for CC interactions and can only be measured through neutral current (NC) interactions. While there are many theoretical models of supernovae collapse, they vary greatly in the prediction and treatment of ν_x [4–6]. With little existing experimental information and large uncertainties in the model space, measurements of NC neutrino interactions will be crucial for understanding the ν_x component of core collapse supernovae. Using recently updated incoherent NC neutrino-nucleus crosssections [7], we provide predictions and sensitivities for average ν_x temperature reconstructions.

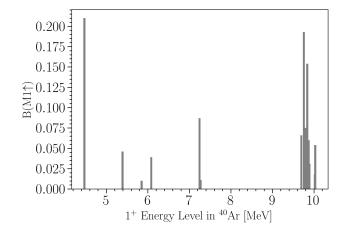


FIG. 1: **B(M1↑)** neutral current 1⁺ transition strengths for ⁴⁰**Ar**. The B(M1↑) value for each 1⁺ is shown as a function of the transition energy. Fourteen of these 1+ transitions exist in total.

II. MEASUREMENT STRATEGY

In the incoherent neutral current interaction, Argon nucleons are excited via interaction with a neutrino. As the nucleon de-excites, γ -rays are emitted at specific energy levels. The magnetic dipole strengths of these 1^+ excited state transitions are displayed in Fig. 1. These measurements, combined with shell model calculations, guide neutral current cross-section predictions and dictate experimental reconstruction of incident neutrino spectra.

Neutral current neutrino-Argon interactions are difficult to measure due to the small cross-section of this channel and low energy at which the interactions occur [7]. For supernovae neutrino energies, the NC interaction cross-section is at least two orders of magnitude smaller than the corresponding CC cross-section, given by [8]. For this reason, projected measurements of supernova neutrinos tend to focus on CC channels.

While NC measurements are difficult to make compared to the CC channel, they provide the only source of information about the neutrino species of ν_x . Flavor non-specific information from supernovae neutrinos is crucial to understanding the neutrino flux emitted without uncertainties related to neutrino oscillations, matter effects, or neutrino self-interactions that occur within the supernovae. Furthermore, measurements of all neutrino species will provide us with a more complete understanding of supernovae neutrinos. Combining flavor non-specific NC measurements with ν_e and $\bar{\nu_e}$ CC measurements, we can indirectly probe the properties of the supernova ν_x flux.

Recent developments in detector technology will allow us to overcome this challenge with ultra-large detectors that are sensitive to these low energy NC interactions. With 40 kt of combined fiducial mass and energy resolution down to the MeV scale, the DUNE Far Detector (FD) modules will be an ideal candidate to study the ν_x component, providing the largest sample of NC neutrino-Argon interactions [9]. DUNE will be able to separate CC from NC interactions using the distribution of deposited energy as a function of interaction length within the detector. The DUNE FD modules are planned to have a high efficiency trigger system down to the few MeV threshold, with good energy resolution, and moderate spatial resolution [9, 10]. With these anticipated capabilities, DUNE will be able to resolve photon emissions from NC interaction in the energy range of interest for this analysis.

While this work is directly relevant to DUNE, SBND, ICARUS and other Liquid Argon (LAr) detectors, supernovae neutrino interaction measurements on other nuclei will provide further insights into the ν_x spectrum. The Jiangmen Underground Neutrino Observatory (JUNO) experiment will be able to observe incoherent neutral current neutrino interactions on Carbon nuclei, with a predominant excitation state of 15.1 MeV [11]. A combined analysis of NC neutrino interactions on 40 Ar and 12 C would provide a robust and uniquely sensitive measurement of ν_x supernovae neutrinos.

In addition to NC measurements, DUNE and Hyper-K will provide leading constraints on the ν_e and $\bar{\nu_e}$ spectrum through CC measurements on liquid Argon and water, respectively. By incorporating DUNE CC, DUNE NC, and Hyper-K CC measurements in a combined analysis, we can make definitive statements about the ν_x component of the neutrino flux. Although sample sizes for NC events are much smaller, and energy resolution is poorer, the information we obtain from NC interaction on Argon nuclei in DUNE provides enough discriminating power to reconstruct the average ν_x temperature.

III. METHODOLOGY

Modelling the neutral current measurements requires three ingredients: the supernova neutrino flux as a function of neutrino temperature, the cross-section of the NC interaction, and DUNE's detector response. Our choices for these three components of the calculation are described below.

We model the supernovae neutrino flux with a Fermi-Dirac spectrum, assuming a progenitor of 10 solar masses at a distance of 10 kpc from Earth as a benchmark. The supernovae neutrino differential flux, as first described by in [12], is given by

$$\frac{dF_{\nu}}{d\varepsilon_{\nu}} = \frac{L_{\nu}}{4\pi D^2 T_{\nu}^4 F_3(\eta)} \frac{\varepsilon_{\nu}^2}{e^{\beta(\varepsilon_{\nu} - \mu)} + 1},\tag{1}$$

where ε_{ν} is incident neutrino energy, L_{ν} is the luminosity for each neutrino species of SN1987A integrated over total time of collapse for a total energy of approximately 3×10^{53} ergs, D is the distance from Earth to the supernova, T_{ν} is the average temperature of the neutrino species, μ is the chemical potential, $\beta = 1/T_{\nu}$, and $\eta = \mu/T_{\nu}$ (the Boltzmann constant is set to unity). $F_3(\eta)$ is defined by

$$F_3(\eta) \equiv \int_0^\infty \frac{x^n}{e^{x-\eta} + 1} dx,\tag{2}$$

and in this work η is set to 0. Fig 2 provides an example of this calculation, setting $T_{\nu_e}=3.3\,\mathrm{MeV},\,T_{\bar{\nu_e}}=4.6\,\mathrm{MeV},$ and $T_{\nu_x}=6.4\,\mathrm{MeV}.$

A pinching parameter can further modify the energy spectrum of supernova neutrinos to closer match the high energy tails of radiated neutrino spectra [1, 4–6]. For measurements of the CC channel, where neutrino energy and observed energy are highly correlated, it is possible to resolve the two parameters the pinched spectrum model and even to differentiate between more complex energy spectra.

The characteristics of the NC channel, however, do not allow for such accurate measurements of the neutrino energy spectrum. Incoherent NC interactions between MeV scale neutrinos and Argon nuclei place the Argon nucleus into one of several excited states. As the Argon nucleus returns to a relaxed state, it emits a γ -ray with discrete energy between 4.47 MeV and 10.03 MeV, corresponding to the specific exited state. While the threshold of these interactions is directly related to the excitation energy, the only other correlation between neutrino energy and observed energy comes from small differences in the crosssections of the different excitation channels. This decoupling of neutrino energy and observed energy results in limited sensitivity to the original neutrino energy spectrum. For this reason, we choose a simple model, the Fermi-Dirac distribution, for the energy spectrum of each flux component. While a pinching parameter can further modify the energy spectrum, this parameter gives

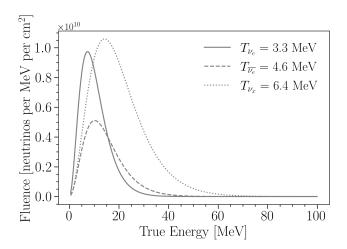


FIG. 2: Supernova neutrino differential fluence for a Fermi-Dirac spectrum. The differential fluence is shown as a function of neutrino energy for each of the three neutrino flux components, assuming a Fermi-Dirac energy distribution, and the baseline supernova scenario described in III.

changes to the flux that are similar in magnitude to changes from the average temperature, and can be degenerate with the average temperature [13]. Therefore this analysis is concerned with using expected NC events to measure average temperature of the neutrino fluence without considering a pinching parameter.

For neutrino interactions on Argon nuclei, we use the most recently published NC cross-sections from W. Tornow et. al. [7] Fig 3 shows this cross-section for neutrinos and anti-neutrinos with 43 % theoretical uncertainty. The uncertainty is composed of 15% uncertainty on the B(M1 \uparrow) measurements, which measure the transition strength of the γ -ray excitations and 40% theoretical uncertainty due to differences derived from choice of shell-model calculation.

We accounted for the uncertainty in the cross-section using a fractional covariance matrix comprised of 15% correlated uncertainties within each excitation mode and 40% uncorrelated uncertainties across the entire energy spectrum. An example of the fractional covariance matrix is displayed in Fig 4. For this analysis, the covariance matrix varies with input neutrino temperatures. To enable reconstruction of ν_x temperature across a wide range of injected temperatures, the fractional covariance matrices were computed at approximately every two MeV of temperature and trilinear interpolation was utilized to generate the necessary fractional covariance matrix.

The final component necessary to model the supernovae signal in DUNE is the detector response and reconstruction efficiency. DUNE expects 15% energy resolution in their TPCs at the energies of relevance for supernovae neutrino measurements [9]. Using this predicted energy resolution and the cross-sections of the individual photon excitation modes, we calculated a response ma-

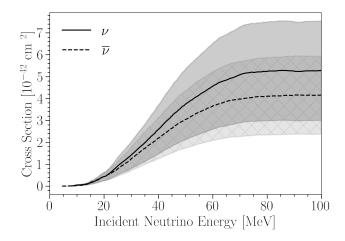


FIG. 3: Incoherent NC neutrino-Argon cross-sections and uncertainties. The

neutral-current neutrino-Argon cross-sections derived in [7] are shown for ν and $\bar{\nu}$ as a function of incident neutrino energy with bands showing their associated 43% uncertainties. The Solid shading ν cross-section uncertainties, and hatched shading shows the same for $\bar{\nu}$

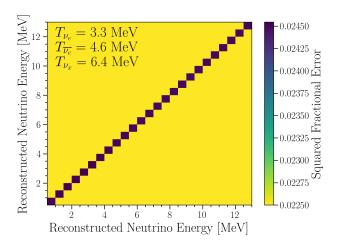


FIG. 4: **DUNE FD NC fractional covariance matrix.** The uncertainties on the cross section are composed of 15% correlated uncertainties and 40% uncorrelated uncertainties, as described in [7]

trix to capture the detector's response to NC events for the ν and $\bar{\nu}$ cross section channels. This response matrix weights each excitation mode proportional to the interaction cross-section for each mode to produce a general response matrix, which we show in Fig. 5.

We further explored efficiency cuts using the distribution of deposited energy per unit distance traveled in the detector to separate NC events from CC events. Using DUNE's expected dE/dx distribution for photon and electron particles, described in [9], we scaled these normalized distributions to the expected event rates in the

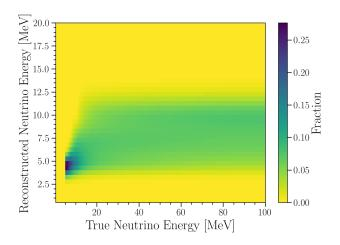


FIG. 5: **DUNE FD NC response matrix.** Response matrix for the ν component of the incoherent NC neutrino interaction in LAr assuming 15% energy resolution for the DUNE FD TPC as described in [9].

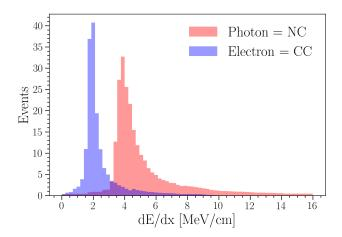


FIG. 6: **DUNE dE/dx distribution for electron** and photon like final states. Distribution is normalized to the expected NC and CC event rates for a representative sample where $T_{\nu_x} = 3.3 \, \text{MeV}$, $T_{\bar{\nu_e}} = 4.6 \, \text{MeV}$, and $T_{\nu_x} = 6.4 \, \text{MeV}$.

NC and CC channels in our reconstructed energy region of interest between 0.5 and 13 MeV for $T_{\nu_e} = 3.3 \,\text{MeV}$, $T_{\bar{\nu_e}} = 4.6 \,\text{MeV}$, and $T_{\nu_x} = 6.4 \,\text{MeV}$, shown in Fig. 6.

We found that one cut in the dE/dx region of 3.1 MeV/cm includes 95.26% of the signal events while rejecting all but 15.83% of the background CC interactions due to the ν_e supernovae neutrino flux that DUNE will also be sensitive to.

Fig. 7 is an example expected reconstructed event rate in DUNE FD, after combining the NC cross-section, response matrix, efficiency cut, and fluence for the specified neutrino temperatures. This plots show the expected events for $T_{\nu_e} = 3.3 \, \text{MeV}$ and $T_{\bar{\nu_e}} = 4.6 \, \text{MeV}$ while average T_{ν_x} varies between 1 MeV and 30 MeV. The dashed

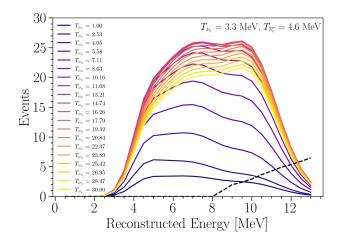


FIG. 7: Expected NC event rate in DUNE FD as a function of ν_x temperature. ν_e and $\bar{\nu_e}$ temperatures are fixed to 3.3 MeV and 4.6 MeV respectively. The black dashed line represents events due to CC interactions in the DUNE FD from the ν_e component of the fluence.

black line represents the CC events due to the ν_e component of the supernovae neutrino flux in DUNE. Although the NC channel is suppressed compared to the CC channel, DUNE's large detector size combined with the high fluence of expected neutrinos for a supernovae collapse provides us with a large enough sample to perform spectral analysis.

The goal of this analysis is to demonstrate reconstruction of the ν_x temperature by combining NC channel measurements from the DUNE FD and constraints on ν_e and $\bar{\nu_e}$ temperatures from CC measurements in DUNE and Hyper-K respectively. DUNE TPCs are predicted to resolve energies in our region of interest to around 15% [9]. Using this energy resolution to calculate the CC response matrix, ν_e fluence described in 1, and CC cross section [8], we calculated the predicted CC event rate as a function of average ν_e temperature in DUNE and were able to reconstruct injected temperatures to 1 sigma credible region with 0.5 % fractional error. We expect that Hyper-K will be able to reconstruct average $\bar{\nu}_e$ temperature to similar precision given their similar energy resolution [14] as the DUNE TPC, greater fiducial mass [15] than the DUNE FD modules, and greater crosssection for inverse beta decay events below $\sim 15\,\mathrm{MeV}$ than ν_e CC events on Argon [16].

IV. STATISTICAL METHODS

With the methods described above, we can now predict the NC event rates in DUNE for any combination of temperatures of the three neutrino flux components. The NC data from DUNE provides information about the total neutrino flux, however, to obtain sensitivity to

the ν_x temperature we must simultaneously constrain the temperature of the ν_e and $\bar{\nu_e}$ components. We construct the binned-log-likelihood comparing expected NC DUNE data to our predictions, and combine this with external statistical constraints on ν_e and $\bar{\nu_e}$. This combination produces a constrained log-likelihood given by

$$\mathcal{L}(\vec{T}) = \left[\prod_{i} \frac{\lambda_{i}(\vec{T}, \alpha_{i})^{k_{i}} e^{-\lambda_{i}(\vec{T}, \alpha_{i})}}{k_{i}!} \right] \mathcal{P}\left(T_{\nu_{e}}\right) \mathcal{P}\left(T_{\bar{\nu_{e}}}\right) \mathcal{P}(\vec{\alpha}),$$
(3)

where $\lambda_i(\vec{T}, \alpha_i)$ is the expected number of events in bin i for the combination of temperatures \vec{T} , and k_i is the number of observed data events in bin i. For the two external constraints, $\mathcal{P}(T_{\nu_e})$ and $\mathcal{P}(T_{\bar{\nu_e}})$, we assume Normally distributed constraints centered on the true values of the temperatures with widths that correspond to the uncertainties on ν_e and $\bar{\nu_e}$ temperatures that we expect to obtain from the CC measurements of DUNE and Hyper-K, assumed to be 0.5%. To model the cross-section uncertainties, we introduce the parameters $\vec{\alpha}$ which fractionally modify the expected number of events in each bin, such that $\lambda_i(\vec{T}, \alpha_i) = (1 + \alpha_i) \cdot \lambda_i(\vec{T})$. The parameters $\vec{\alpha}$ are constrained by the multivariate normal distribution denoted by $\mathcal{P}(\vec{\alpha})$, which has a fractional covariance matrix derived from the cross-section uncertainties.

To explore the sensitivity of this combined analysis to the ν_x average temperature, we examine a set of representative scenarios where $T_{\nu_e} = 3.3 \,\text{MeV}, T_{\bar{\nu_e}} = 4.6 \,\text{MeV},$ and T_{ν_x} has a value between 0.5 MeV and 30 MeV. For each value of T_{ν_x} we perform an Asimov test, where the nominal expected event distribution is injected as data We use a Markov Chain Monte Carlo with adaptive parallel tempering [17, 18] to explore the parameter space, and derive Bayesian credible regions (CR) for T_{ν_x} that are marginalized over T_{ν_e} , $T_{\bar{\nu_e}}$, and the nuisance parameters $\vec{\alpha}$. The two electron flavor temperatures have normal priors modeled after the expected constraints from CC data, and the nuisance parameters $\vec{\alpha}$ have a multivariatenormal prior, as described in 3. We use a uniform prior for T_{ν_x} across most of the parameter space, but introduce a hyperbolic tangent cutoff at 60 MeV, with a characteristic transition width of 3 MeV. For injected $T_{\nu_{\alpha}}$ less than 10 MeV a degenerate region of the parameter space becomes apparent, which extends to reconstructed temperatures above 100 MeV for the lowest injected temperatures. We focus the results presented here on temperatures below 60 MeV, because such large temperatures are not within the expected range, and will be ruled out by other observations [19–24]. This is accomplished with the hyperbolic tangent cutoff, the primary effect of which is a reduction in the size of the derived CR's for injected T_{ν_x} less than 5 MeV, because there is no longer appreciable posterior mass above 60 MeV. Additional discussion of this prior, and CR's derived with a uniform T_{ν_x} prior from 0.1 MeV to 300 MeV are given in Appendix A.

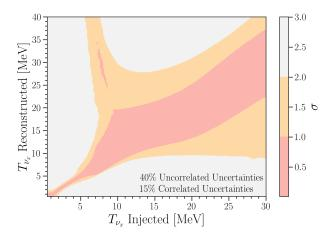


FIG. 8: Expected T_{ν_x} credible regions with full cross-section uncertainties. The Asimov credible regions for T_{ν_x} are shown as a function of injected T_{ν_x} by the colored regions. Average neutrino temperatures of $T_{\nu_e} = 3.3\,\mathrm{MeV}$ and $T_{\bar{\nu_e}} = 4.6\,\mathrm{MeV}$ are assumed, along with 40% uncorrelated uncertainties and 15% correlated uncertainties on the NC cross-section.

V. RESULTS

The average ν_e and $\bar{\nu_e}$ temperatures will be constrained very well by CC measurements from DUNE and Hyper-K. As a result, the sensitivity to T_{ν_x} does not significantly depend on the choice of injected T_{ν_e} and $T_{\bar{\nu_e}}$. We can therefore examine the sensitivity to reconstructed ν_x temperature as a function of true injected ν_x temperature without significant bias from the choice of injected ν_e and $\bar{\nu_e}$ temperatures. We present sensitivities to T_{ν_x} , using $T_{\nu_e}=3.3\,\mathrm{MeV}$ and $T_{\nu_e}=4.6\,\mathrm{MeV}$ as a representative set of temperatures.

We explore sensitivities for three scenarios with different cross-section uncertainties: a case without cross-section uncertainties, at case with full cross-section uncertainties. The case with full cross-section uncertainties. The case with full cross-section uncertainties assumes 40 % fully uncorrelated uncertainty in the cross-section and a 15 % correlated uncertainty in the cross-section as described in III. The case with reduced cross-section uncertainties retains the 40 % fully uncorrelated uncertainty, but reduces the correlated uncertainty to 7 % to model the effect of improved B(M1 \uparrow) measurements. Fig. 10, 8, and 9 show the expected sensitivity to T_{ν_x} as Asimov credible regions for the no uncertainties, full uncertainties, and reduced uncertainties cases respectively.

There are two distinct degenerate regions that arise in the measurement space from multiple factors. The primary cause is the discrete γ -ray energies of the NC cross-section that results in a decoupling between neutrino energy and observed energy. In addition to that, for T_{ν_x} above approximately 8 MeV the total fluence becomes much more uniform across the energy range of the NC

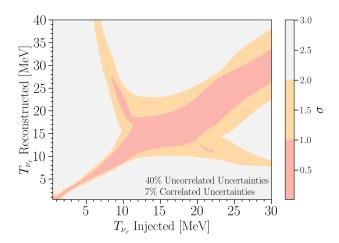


FIG. 9: Expected T_{ν_x} credible regions with reduced cross-section uncertainties. The Asimov credible regions for T_{ν_x} are shown as a function of injected T_{ν_x} by the colored regions. Average neutrino temperatures of $T_{\nu_e} = 3.3 \,\text{MeV}$ and $T_{\bar{\nu_e}} = 4.6 \,\text{MeV}$ are assumed, along with 40% uncorrelated uncertainties and 7% correlated uncertainties on the NC cross-section.

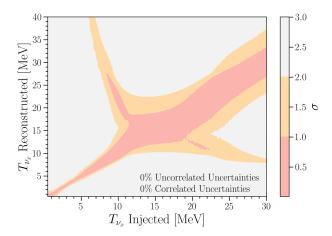


FIG. 10: Expected T_{ν_x} credible regions with no cross-section uncertainties. The Asimov credible regions for T_{ν_x} are shown as a function of injected T_{ν_x} by the colored regions. Average neutrino temperatures of $T_{\nu_e} = 3.3\,\mathrm{MeV}$ and $T_{\bar{\nu_e}} = 4.6\,\mathrm{MeV}$ are assumed, along no uncertainties on the NC cross-section.

excitations. These characteristics of the NC cross-section combined with the Fermi-Dirac spectrum at higher average temperatures leads to a degeneracy in the ν_x temperature measurement.

Fig. 11 shows the fractional width of the 1σ credible region for these measurements. The peak in the fractional width of the 1σ credible region around 10 MeV true ν_x temperature is due to the degeneracy in the measurement. Reducing the correlated uncertainties from 15% to 7%, without changes to the 40% uncorrelated uncer-

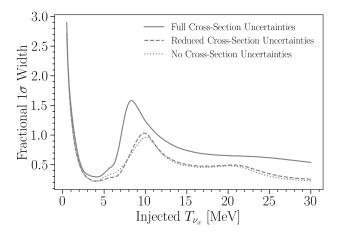


FIG. 11: Fractional width of the 1σ credible region. Solid line represents the scenario with 40% uncorrelated uncertainties and 15% correlated uncertainties on the NC cross-section. Dashed line represents the scenario with 40% uncorrelated uncertainties and 7% correlated uncertainties on the NC cross-section. Dotted line represents the scenario with no uncertainties on the NC cross-section.

tainties, reduces the fractional width of the 1σ credible region almost to that of the measurement without any uncertainties on the cross section. This demonstrates that even modest improvements to the Argon B(M1 \uparrow) measurements provide substantial improvements to the T_{ν_x} sensitivity.

VI. CONCLUSIONS

While NC channel measurements are often overlooked due to the technical challenges and small sample sizes, this analysis has shown the power of NC measurements in measuring ν_x spectral information from Type-II core collapse supernovae events. Due to the discrete excitation nature of this interaction channel, the energy spectrum from supernovae neutrinos cannot be resolved, but general parameters of the fluence can be measured to the 1σ and 2σ level. For this analysis we focused on measuring the average ν_x temperature from the incoherent NC neutrino-Argon interaction in the DUNE FD modules. To make this measurement we combined the expected incoherent NC sample from the DUNE FD with expected constraints from the CC channel measurements of the DUNE and Hyper-K experiments on $T\nu_e$ and $T_{\bar{\nu}_e}$ of the supernovae flux. We find that such a combined analysis can measure the average ν_x temperature to within a factor of two in most cases, and to within 30% in the best

In addition to exploring DUNE's sensitivity to average ν_x temperature using the NC channel, we explore the effects of reducing the uncertainty in NC cross-section pre-

dictions. By reducing correlated uncertainties from 15% to 7%, the T_{ν_x} measurement becomes sample size limited, and approaches the case where there are no uncertainties on the cross-section. More precise measurements of B(M1 \uparrow) transition strengths will provide even greater spectral information for the ν_x component of supernovae flux. While this measurement will be limited by small energy range of Argon-nucleus gamma emissions from NC interactions, combining NC measurements of neutrinos on Argon with NC measurements of neutrinos on Carbon from JUNO could provide stronger constraints on average ν_x temperature reconstruction.

VII. ACKNOWLEDGEMENTS

We want to thank Janet M. Conrad for insights on liquid Argon TPCs. We would also like to thank Anna C. Hayes for her dedicated work on modeling neutral current cross-sections. DAN is supported by the NSF Graduate Research Fellowship under Grant No. 2141064. AS is supported by the U.S. Department of Energy through the Los Alamos National Laboratory. Los Alamos National Laboratory is operated by Triad National Security, LLC, for the National Nuclear Security Administration of U.S. Department of Energy (Contract No. 89233218CNA000001).

- A. Mirizzi, I. Tamborra, H.-T. Janka, N. Saviano, K. Scholberg, R. Bollig, L. Hudepohl, and S. Chakraborty, Riv. Nuovo Cim. 39, 1 (2016), 1508.00785.
- [2] A. A. Abud et al. (DUNE Collaboration) (2023), 2303.17007.
- [3] K. Abe et al. (Hyper-Kamiokande), Astrophys. J. 916, 15 (2021), 2101.05269.
- [4] G. G. Raffelt, Astrophys. J. 561, 890 (2001), astroph/0105250.
- [5] G. G. Raffelt, M. T. Keil, R. Buras, H.-T. Janka, and M. Rampp, in 4th Workshop on Neutrino Oscillations and their Origin (NOON2003) (2003), pp. 380–387, astro-ph/0303226.
- [6] R. Buras, H.-T. Janka, M. T. Keil, G. G. Raffelt, and M. Rampp, Astrophys. J. 587, 320 (2003), astroph/0205006.
- W. Tornow, A. P. Tonchev, S. W. Finch, Krishichayan,
 X. B. Wang, A. C. Hayes, H. G. D. Yeomans, and D. A.
 Newmark, Phys. Lett. B 835, 137576 (2022), 2210.14316.
- [8] M. Bhattacharya, C. D. Goodman, and A. García, Phys. Rev. C 80, 055501 (2009), URL https://link.aps.org/doi/10.1103/PhysRevC.80.055501.
- [9] B. Abi et al. (DUNE) (2020), 2002.03005.
- [10] F. Cavanna, Personal communication (2022).
- [11] Z. Djurcic et al. (JUNO) (2015), 1508.07166.
- [12] T. Totani, K. Sato, H. E. Dalhed, and J. R. Wilson, Astrophys. J. 496, 216 (1998), astro-ph/9710203.
- [13] H. Minakata, H. Nunokawa, R. Tomas, and J. W. F. Valle, JCAP 12, 006 (2008), 0802.1489.
- [14] N. F. Bell, M. J. Dolan, and S. Robles, JCAP 09, 019 (2020), 2005.01950.
- [15] K. Abe et al. (Hyper-Kamiokande) (2018), 1805.04163.
- [16] K. Scholberg, Ann. Rev. Nucl. Part. Sci. 62, 81 (2012), 1205.6003.
- [17] D. Foreman-Mackey, D. W. Hogg, D. Lang, and J. Good-man, Publ. Astron. Soc. Pac. 125, 306 (2013), 1202.3665.
- [18] W. D. Vousden, W. M. Farr, and I. Mandel, Monthly Notices of the Royal Astronomical Society 455, 1919 (2015), URL https://doi.org/10.1093/mnras/stv2422.
- [19] J. F. Beacom, Ann. Rev. Nucl. Part. Sci. 60, 439 (2010), 1004.3311.
- [20] S. E. Woosley and W. C. Haxton, Nature **334**, 45 (1988).
- [21] M. T. Keil, G. G. Raffelt, and H.-T. Janka, Astrophys. J. 590, 971 (2003), astro-ph/0208035.

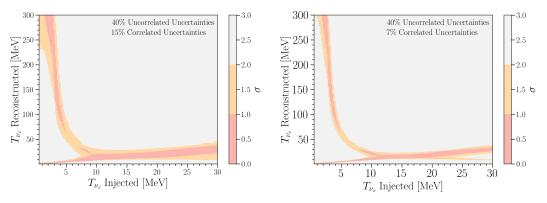
- [22] T. Yoshida, T. Kajino, and D. H. Hartmann, Phys. Rev. Lett. 94, 231101 (2005), astro-ph/0505043.
- [23] A. Heger, E. Kolbe, W. C. Haxton, K. Langanke, G. Martinez-Pinedo, and S. E. Woosley, Phys. Lett. B 606, 258 (2005), astro-ph/0307546.
- [24] H. Yuksel, S. Ando, and J. F. Beacom, Phys. Rev. C 74, 015803 (2006), astro-ph/0509297.

Appendix A: T_{ν_x} Prior

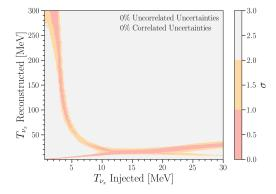
In this work we demonstrate the potential sensitivity of the DUNE FD to the average temperature of the supernova ν_x component with credible regions derived from the highest posterior density regions (HPD). A side effect of this methodology is a dependence of the local HPD width on the global distribution of posterior mass. For these NC derived constraints on T_{ν_x} , a degenerate region of allowed ν_x temperatures is present for the entire energy range. Below $\sim 10\,\mathrm{MeV}$ and above $\sim 20\,\mathrm{MeV}$, this degeneracy manifests as two distinct allowed regions at both the 1σ and 2σ level. For some values of injected T_{ν_x} the allowed region not centered on the injected temperature, referred to as the degenerate region, lies within the range of expected supernova neutrino temperatures. However, for injected T_{ν_x} less than $\sim 5\,\mathrm{MeV}$ this degenerate region exists at temperatures far above the expected range of supernova neutrino temperatures. In the main text of this paper, we choose to apply a prior that allows only values of T_{ν_x} below 60 MeV. This is motivated by the low temperatures observed from SN1987A [20], predicted by supernova simulation studies [21], required by constraints from neutrino induced nucleosynthesis [22, 23], and disfavored by diffuse supernova background searches [24]. This results in expected sensitivities that are not biased by a degeneracy that is both far outside of the range of expected supernova behavior and which would be ruled out by other measurements.

In this appendix we show the expected sensitivities under a different prior assumption, namely a uniform prior on T_{ν_x} between 0.1 MeV and 300 MeV. Because the degenerate region extends above 60 MeV at low ν_x temperatures and contains appreciable posterior mass, this has the effect of widening the allowed regions of T_{ν_x} that are centered on the injected T_{ν_x} . Fig. 12 show the expected sensitivity to T_{ν_x} with this wider range of allowed T_{ν_x} values for the three different cross-section uncertainty scenarios explored in the main text. The degenerate region below $\sim 5\,\mathrm{MeV}$ extends up into the 100's of MeV, and below $\sim 3\,\mathrm{MeV}$ the degenerate region begins to intersect with the prior boundary at 300 MeV.

To examine the effect of this prior we compare the width of the 1σ credible region across three scenarios: the full width derived from a uniform T_{ν_x} prior between 0.1 MeV and 300 MeV, the width of the allowed region below 60 MeV using the same uniform T_{ν_x} prior between 0.1 MeV and 300 MeV, and finally the width derived using the prior from the main text (a hyperbolic-tangent cutoff prior that penalizes T_{ν_x} above 60 MeV and has a 3 MeV characteristic width). Fig. 13 shows the fractional width of these 1σ credible regions for the three scenarios. The solid lines denote the case where T_{ν_x} prior is in the form of a hyperbolic tangent cutoff at 60 MeV. Relaxing the prior assumptions on T_{ν_x} significantly widens the allowed regions below 60 MeV for injected T_{ν_x} between 1 MeV and 5 MeV, but does not significantly effect the expected allowed regions outside of this region. The width of the allowed regions considering the full T_{ν_x} parameter space up to 300 MeV remains largely unchanged outside of this 1 MeV to 5 MeV region of injected T_{ν_x} , but between 1 MeV and 5 MeV is dominated by the large width of the high-temperature degenerate region.



(a) 40% uncorrelated uncertainties and 15% correlated (b) 40% uncorrelated uncertainties and 7% correlated uncertainties on the NC cross-section uncertainties on the NC cross-section



(c) No uncertainties on the NC cross-section

FIG. 12: Expected T_{ν_x} credible regions with a uniform prior from $0.1\,\mathrm{MeV}$ to $300\,\mathrm{MeV}$. The Asimov credible regions for T_{ν_x} are shown as a function of injected T_{ν_x} by the colored regions. Average neutrino temperatures of $T_{\nu_e} = 3.3\,\mathrm{MeV}$ and $T_{\bar{\nu_e}} = 4.6\,\mathrm{MeV}$ are assumed. The credible regions in this figure are computed with a uniform T_{ν_x} prior that extends up $300\,\mathrm{MeV}$; this is in contrast to the credible regions shown in Figures 8, 9, 10 which limited values of T_{ν_x} to be below $60\,\mathrm{MeV}$.

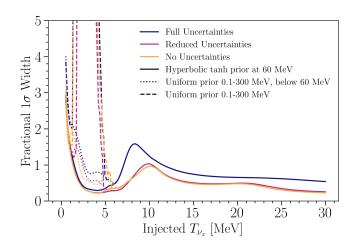


FIG. 13: Fractional width of 1σ credible regions. The solid lines correspond to the width from the hyperbolic tangent prior, the dotted lines correspond to the width below $60\,\mathrm{MeV}$ from the $0.1-300\,\mathrm{MeV}$ uniform prior, and the dashed lines correspond to the full width from the from the $0.1-300\,\mathrm{MeV}$ uniform prior (which extends up to 35). The three colors correspond to the three cases of cross section uncertainties.